

# Near Infrared Spectra of the Orion Bar

A. Marconi<sup>1,3</sup>, L. Testi<sup>1,4</sup>, A. Natta<sup>2</sup>, and C.M. Walmsley<sup>2</sup>

<sup>1</sup> Dipartimento di Astronomia e Scienza dello Spazio, Università degli Studi di Firenze, Largo E.Fermi 5, I-50125 Firenze, Italy

<sup>2</sup> Osservatorio Astrofisico di Arcetri, Largo E.Fermi 5, I-50125 Firenze, Italy

<sup>3</sup> Space Telescope Science Institute, 3700 San Martin Drive, Baltimore, MD 21218

<sup>4</sup> Division of Physics Mathematics and Astronomy, Caltech, MS 105-24, Pasadena, CA 91125, USA

Received date; accepted date

**Abstract.** We have used the LONGSP spectrometer on the 1.5-m TIRGO telescope to obtain long slit spectra in the J, H, and K wavelength bands towards two positions along the Orion bar. These data have been supplemented with images made using the ARNICA camera mounted on TIRGO as well as with an ESO NTT observation carried out by Dr A. Moorwood. We detect a variety of transitions of hydrogen, helium, OI, FeII, FeIII, and H<sub>2</sub>. From our molecular hydrogen data, we conclude that densities are moderate ( $3 - 6 \times 10^4 \text{ cm}^{-3}$ ) in the layer responsible for the molecular hydrogen emission and give no evidence for the presence of dense neutral clumps. We also find that the molecular hydrogen bar is likely to be tilted by  $\sim 10$  degrees relative to the line of sight. We discuss the relative merits of several models of the structure of the bar and conclude that it may be split into two structures separated by 0.2-0.3 parsec along the line of sight. It also seems likely to us that in both structures, density increases along a line perpendicular to the ionization front which penetrates into the neutral gas.

We have used the  $1.317 \mu\text{m}$  OI line to estimate the FUV radiation field incident at the ionization front and find values of  $1 - 3 \times 10^4$  greater than the average interstellar field. From [FeII] line measurements, we conclude that the electron density in the ionized layer associated with the ionization front is of order  $10^4 \text{ cm}^{-3}$ . Finally, our analysis of the helium and hydrogen recombination lines implies essential coincidence of the helium and hydrogen Strömgen spheres.

**Key words:** interstellar medium: HII regions – interstellar medium : Orion – IR: interstellar medium : lines and bands

## 1. Introduction

The properties of the Orion nebula are the starting point for many of our ideas on high mass stars and their interactions with the environment. A symposium held in 1981 (Glassgold et al. 1982) summarises much of what was known at that time. More recent work has been reviewed by Genzel & Stutzki (1989). In general, the aim has been to understand the ionization structure and dynamical evolution of the nebula. In recent years, much attention has been paid to the hot neutral gas adjacent to the ionization front known as a PDR or Photon Dominated Region.

Work on the ionized nebula has tended to concentrate upon determinations of the ionization structure and elemental abundances (see Peimbert 1982, Simpson et al. 1986). More recent optical and infrared studies have been carried out by Osterbrock et al. (1990, 1992), Baldwin et al. (1991), Peimbert et al. (1992), Pogge et al. (1992), De Poy & Pogge (1994), Bautista et al. (1995), Rubin et al. (1993), and Rodriguez (1996). A review of the results has been made by Peimbert (1993) and discussions of the methods employed are given by Mathis (1995) and by Peimbert (1995). These studies in general indicate that the major fraction of elements such as C,N,O,S are in the gas phase within the ionized nebula whereas species such as Si and Fe appear to be depleted by roughly an order of magnitude relative to abundances either in the Sun or nearby B stars.

Radio work on Orion has revealed an immense variety of structures in the emissions of the ionized gas ( e.g. Felli et al. 1993, Yusuf-Zadeh 1990). Particularly striking is the bar-like structure situated roughly 2 arc minutes (0.25 parsec) to the south-east of the Trapezium stars which is the subject of this article. “The Bar” is also observed in molecular line emission (see below) and clearly marks an ionization front where Lyman continuum photons from the O6 star  $\Theta^1\text{C Ori}$  are absorbed. The dynamical behavior of the ionized gas can be studied in radio recombination lines (Pankonin et al. 1979, Wilson & Jäger 1987, Wilson & Filges 1990, Wilson et al. 1997) from which one

concludes that much of the ionized material in Orion is streaming towards the observer.

Infrared studies of HII regions sample not only the ionized gas but also the adjacent neutral material or PDR. A recent review of the properties of these regions is that of Hollenbach & Tielens (1997) (see also the discussions of Genzel 1992, and Walmsley 1997). Modelling studies have been carried out by Tielens & Hollenbach (1985), Hollenbach et al. (1991), Sternberg & Dalgarno (1989; 1995), Fuente et al. (1993), Jansen et al. (1995a,b), Bertoldi & Draine (1996) and Draine & Bertoldi (1996). Much of this activity has centred on attempts to understand the properties of "The Bar" mentioned above. Recent observational studies using a variety of molecular tracers have been carried out by Tielens et al. (1993), by Tauber et al. (1994; 1995), by Hogerheijde et al. (1995), and by van der Werf et al. (1996). These show a stratification along the direction of the perpendicular to the bar in the plane of the sky. This is in the sense expected for gas heated by the Trapezium stars and consistent according to the models with attenuation by a gas of density  $5 \cdot 10^4 \text{ cm}^{-3}$ . However, the data also seem to show that the gas in the bar is far from homogeneous and that clumps of density as high as  $10^6 \text{ cm}^{-3}$  are embedded in the filament. Such high density condensations presumably either have been or will be soon overrun by the ionization front and will give rise to dense ionized globules within the HII region (see e.g. Lizano et al. 1996, Dyson et al. 1995). Understanding the characteristics of such high density clumps may thus be of critical importance for the evolution of the HII region.

One of the most useful tracers of PDR's has turned out to be the near infrared lines of molecular hydrogen. For example, van der Werf et al. used the FAST camera on the ESO/MPI 2.2 m telescope to image the  $\text{H}_2$   $v = 1 \rightarrow 0$  S(1) ( $2.122 \mu\text{m}$ ) and  $v = 2 \rightarrow 1$  S(1) ( $2.248 \mu\text{m}$ ) lines towards the bar with  $1.5''$  resolution. These show that the transition from atomic to molecular hydrogen in the bar occurs 15 arc seconds ( $0.03 \text{ pc}$  at a distance of  $450 \text{ pc}$ ) to the SE of the ionization front (i.e. away from the ionizing stars). Van der Werf et al. also find that the ratio  $R_{12}$  of the intensities of the  $1 \rightarrow 0$  and  $2 \rightarrow 1$  lines varies between a value of  $8.1 \pm 0.7$  at the peak of the  $\text{H}_2$  emission to a value of  $3.4 \pm 1.9$   $30''$  from the ionization front on the side shielded from the radiation of the Trapezium stars. The latter value is characteristic of UV-pumped fluorescent emission in a low density gas (Sternberg and Dalgarno 1989).

The present study had as its aim to obtain near IR spectra of the gas in the vicinity of the bar in order to verify and extend understanding of the physical conditions on both sides of the ionization front. We were partly motivated by the idea that there is a link between the ionized and PDR components in that the former is mainly sensitive to the radiation just shortward of  $912 \text{ \AA}$  while the latter is basically a measure of the radiation longward of

this limit (see Bertoldi & Draine 1996 for a discussion). It is thus of considerable interest to compare the two using the same instrument. We therefore used the TIRGO telescope on the Gornergrat (Switzerland) to obtain slit spectra in the J, H, and K bands at 3 positions in the vicinity of the bar, shown in Fig. 1. As supplementary information, we also made use of unpublished observations carried out using the IRSPEC spectrometer on the ESO NTT telescope by Dr A.Moorwood.

We summarize in the next section the techniques used for observations and data reductions. The results are presented in Sect.3 and discussed in Sect. 4. We summarize our conclusions in Sect. 5.

## 2. Observations

### 2.1. ARNICA Observations

The Orion Bar was observed during two observing runs in January 1996 and February 1997 using ARNICA (ARcetri Near Infrared CAmera) mounted on the 1.5m TIRGO<sup>1</sup> telescope. ARNICA is equipped with a  $256 \times 256$  NICMOS3 array, the pixel size with the optics used at TIRGO is  $0.96''$ ; for a complete description of the instrument and of its performance, see Lisi et al. (1996) and Hunt et al. (1996). The Bar was imaged in the three J, H, and K broad band filters (centered at  $1.25$ ,  $1.65$ , and  $2.2 \mu\text{m}$ , respectively) and in the  $\text{Br}\gamma$  narrow band filter ( $\lambda = 2.166 \mu\text{m}$ ,  $\Delta\lambda/\lambda \sim 1\%$ , Vanzi et al. 1997b). The seeing was approximately  $2\text{-}3''$  and the observed field was approximately  $\sim 4'.5 \times 4'.5$ , covering all the Bar region. Data reduction was carried out using the IRAF<sup>2</sup> and ARNICA<sup>3</sup> (Hunt et al. 1994) software packages. Photometric calibration in the J, H and K bands was performed by observing photometric standard stars from the list of Hunt et al. (1997); the calibration accuracy is estimated to be  $\sim 5\%$ . The  $\text{Br}\gamma$  image was continuum subtracted and calibrated using the K band image. We show in Fig. 1 (left panel) an image obtained combining the J, H, and K images and (right panel) the continuum subtracted  $\text{Br}\gamma$  image.

### 2.2. LONGSP Observations

J ( $1.25\mu\text{m}$ ), H( $1.65 \mu\text{m}$ ), and K ( $2.2\mu\text{m}$ ) band spectra of the Orion Bar were obtained using the LonGSp (Longslit Gornergrat Spectrometer) spectrometer mounted at the Cassegrain focus on the TIRGO telescope. The spectrometer is equipped with cooled reflective optics and a grat-

<sup>1</sup> The TIRGO telescope is operated by the C.A.I.S.M.I.-C.N.R Firenze, Italy

<sup>2</sup> IRAF is made available to the astronomical community by the National Optical Astronomy Observatories, which are operated by AURA, Inc., under contract with the U.S. National Science Foundation

<sup>3</sup> A description of ARNICA can be obtained from the Arcetri Observatory at <ftp://150.217.20.1/pub/arnica/>

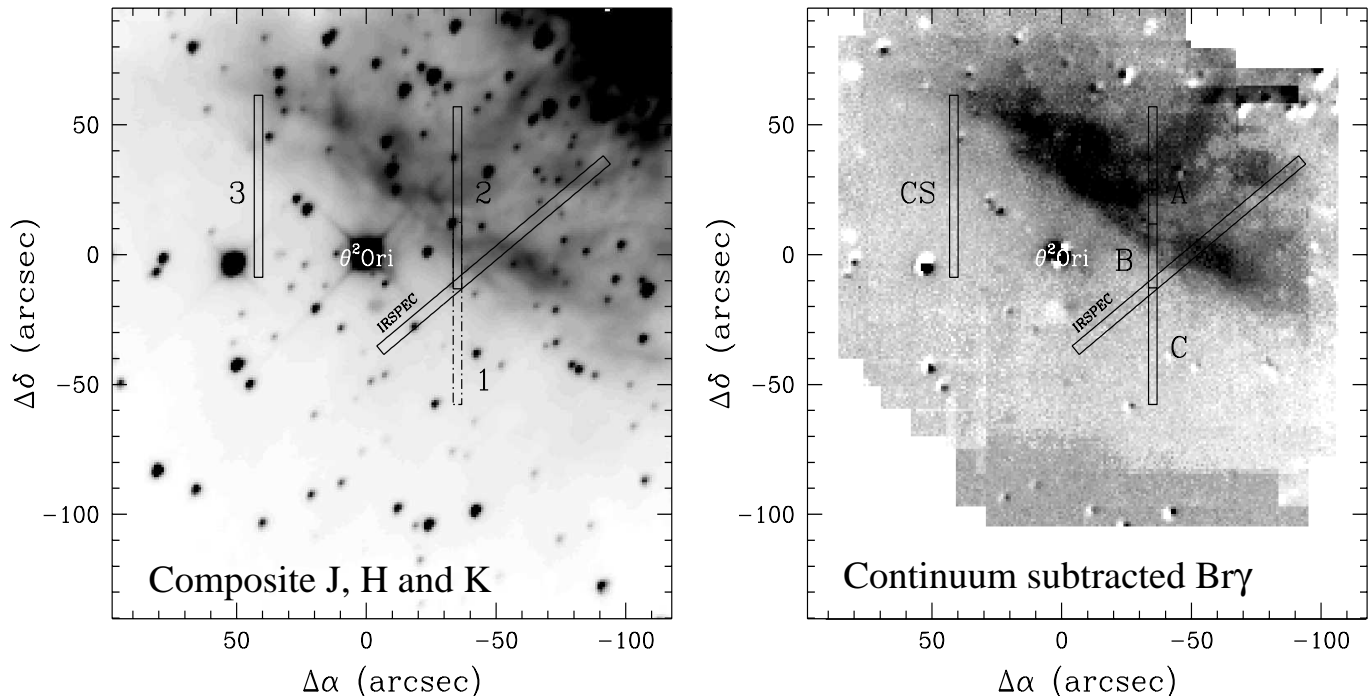


**Fig. 1.** On the left: composite J, H, and K image of the Orion Bar region showing the slit positions used for the LONGSP and IRSPEC observations. Coordinates are offsets in right ascension and declination relative to the position of the star  $\Theta^2$  Ori (R.A.(1950) =  $5^h 32^m 55.^s 5$ , Dec.(1950) =  $-5^\circ 26' 51''$ ). We show our three slit positions (1, 2, and 3) as well as the four positions for which we tabulate line intensities (A, B, C, CS). On the right: Br $\gamma$  image of the Orion Bar region.

ing in Littrow configuration. The detector is a  $256 \times 256$  engineering grade NICMOS3 array (for detector performances see Vanzi et al. 1995). The pixel sizes are  $11.5 \text{ \AA}$  (first order) and  $1''.73$  in the dispersion and slit directions, respectively. LONGSP operates in the range  $0.9\text{--}2.5 \text{ \mu m}$  achieving a spectral resolution at first order of  $R \simeq 550$  in J, 700 in H and 950 in K. For a more comprehensive description of the instrument, refer to Vanzi et al. (1997a).

Observations were conducted in two runs in January and March 1996 under non-photometric conditions. The slit used had dimensions  $3''.5 \times 70''$  and was oriented N-S. The seeing during the observations was in the range  $2''\text{--}4''$ . The Orion Bar was observed at three slit positions labeled as 1, 2, 3 and shown in Fig. 1 superimposed on a NIR image obtained by co-adding the J, H and K ARNICA observations discussed in the previous section. Position 1 and 2 were chosen in order to study the variation of line intensities along a cut encompassing all the bar. Position 3 was subsequently chosen to be coincident with the CS peak discovered by van der Werf et al. at R.A. =  $5^h 32^m 58.5^s$  and Dec. =  $-5^\circ 26' 25''$  (B1950.0). This high density ( $10^6 \text{ cm}^{-3}$ ) clump appears to be illuminated directly from the Trapezium and we thought it useful to examine directly the relative variations in line intensities across the clump. The center of the slits were offset by  $-35''$ ,  $-23''$  (Pos. 1)  $-35''$ ,  $23''$  (Pos. 2) and  $42''$ ,  $26''$  (Pos. 3) in R.A. and Dec. with respect to the star  $\theta^2$  A Ori.

At each grating position we performed 5 ABBA cycles (A=on source, B=on sky) with an on-chip integration time of 60 sec, for a total of 10 min integration on source. At the beginning or at the end of the five cycles on the object we performed 1 ABBA cycle on the O6 star BS 1895 ( $\Theta^1$ C Ori).

Data reduction was performed with the ESO package MIDAS, within the context IRSPEC, modified to take into account LonGSp instrumental characteristics. The frames were corrected for bad pixels, flat-fielded, sky subtracted and wavelength calibrated using the OH sky lines present on all the frames (Oliva & Origlia 1992). After a direct subtraction, sky removal was optimized by minimizing the standard deviation in selected areas where the OH sky lines were poorly subtracted but no object emission was present. The wavelength calibration was performed to better than  $1/5$  of a pixel ( $\simeq 2 \text{ \AA}$ ).

The spectra were then corrected for telluric absorption by dividing by the featureless spectrum of  $\Theta^1$ C Ori. For more details on LonGSp data reduction, see Vanzi et al. 1997a.

Flux calibration of the spectra in the J, H, and K bands was achieved by rescaling the observed flux distribution along the slit to match that obtained from the ARNICA images at the positions of the slits. We consider such calibration accurate to  $\simeq 20\%$  when comparing the fluxes of lines measured in two different bands. Indeed, the

**Table 1.** Spectra in the J, H and K bands

Line	$\lambda$ ( $\mu\text{m}$ )	<i>A</i>	<i>B</i>	<i>C</i>	<i>CS</i>
[OI] $2p^33D - 2p^33P$	1.129	3.6	4.7	6.8	12
[PII] $3p^2D_2 - 3p^2P_2$	1.189	2.4	3.5	3.2	6.6
HeI $5^3D - 3^3P^\circ$	1.197	5.1	5.4	6.0	5.4
HeI $4^3P^\circ - 3^3S$	1.253	6.9	5.9	5.3	2.3
[FeII] $4sa^4D_{7/2} - 4sa^6D_{9/2}$	1.257	4.8	8.3	6.7	18
??	1.268	2.3	1.5	<1.8	5.7
HeI $5^3F^\circ - 3^3D$	1.278	18	16	18	26
HI 5-3	1.282	370	400	450	430
HeI $5^3P^\circ - 3^3D$	1.298	2.2	2.3	1.6	<2.6
+ [FeII] $4sa^4D_{3/2} - 4sa^6D_{1/2}$					
[OI] $2p^34S - 2p^33P$	1.317	3.3	6.8	7.4	8.4
[FeII] $4sa^4D_{7/2} - 4sa^6D_{7/2}$	1.321	1.1	2.3	<1.6	4.7
HeI $5^1S - 3^1P^\circ$	1.341	1.5	1.3	1.6	2.3
HI 21-4	1.514	3.3	2.7	2.7	3.0
HI 20-4	1.520	3.6	3.6	3.6	3.9
HI 19-4	1.526	4.4	4.3	4.5	4.4
HI 18-4	1.534	6.4	6.2	6.6	8.7
+ [FeII] $4sa^4D_{5/2} - 3d^7a^4F_{9/2}$					
HI 17-4	1.544	6.5	5.9	6.3	6.2
HI 16-4	1.556	8.2	7.3	7.2	7.2
HI 15-4	1.570	9.4	9.0	8.2	9.4
HI 14-4	1.588	11	10	10	13
[FeII] $4sa^4D_{3/2} - 3d^7a^4F_{7/2}$	1.600	0.5	0.6	0.9	3.0
HI 13-4	1.611	14	13	13	16
HI 12-4	1.641	18	17	17	19
[FeII] $4sa^4D_{7/2} - 3d^7a^4F_{9/2}$	1.644	5.9	11	8.7	24
[FeII] $4sa^4D_{5/2} - 3d^7a^4F_{7/2}$	1.677	0.8	1.1	<1.1	2.3
HI 11-4	1.681	21	21	23	24
HeI $4^3D - 3^3P^\circ$	1.701	9.1	8.5	8.6	6.4
HeI $10^1P^\circ - 4^1D$	1.732	0.5	1.0	2.1	1.2
HI 10-4	1.737	26	28	29	30
HeI $7^3P^\circ - 4^3S$	1.746	0.9	1.8	3.0	3.9
+ H <sub>2</sub> (1,0)S(7)					
H <sub>2</sub> (1,0)S(6)	1.788	1.5	1.1	1.6	2.2
H <sub>2</sub> (1,0)S(2)	2.034	0.6	....	....	4.9
HeI $2^1P^\circ - 2^1S$	2.058	99	110	74	95
H <sub>2</sub> (2,1)S(3)	2.073	<0.5	1.2	3.6	4.2
HeI $4S - 3^3P^\circ$	2.113	4.2	3.7	2.8	2.1
H <sub>2</sub> (1,0)S(1)	2.122	1.5	5.1	17	15
H <sub>2</sub> (2,1)S(2)	2.154	<0.1	0.2	1.3	1.3
HeI $7F^\circ - 4^1D$	2.162	3.0	2.5	2.4	1.9
HI 7-4	2.166	100	100	100	100
??+H <sub>2</sub> (3,2)S(3)	2.199	0.5	0.9	1.4	3.5
[FeIII] $3d^6G_5 - 3D^6H_6$	2.219	1.4	2.0	1.3	2.3
H <sub>2</sub> (1,0)S(0)	2.223	0.5	1.6	6.6	6.5
[FeIII] $3d^6G_4 - 3d^6H_4$	2.242	0.7	0.6	0.6	0.4
H <sub>2</sub> (2,1)S(1)	2.248	0.4	1.2	4.1	3.8
??+H <sub>2</sub> (3,2)S(2)	2.286	0.7	0.6	1.0	1.4

Note: Intensity 100 corresponds to:

- A )  $2.65 \times 10^{-3} \text{ erg cm}^{-2} \text{ s}^{-1} \text{ sr}^{-1}$
- B )  $2.08 \times 10^{-3} \text{ erg cm}^{-2} \text{ s}^{-1} \text{ sr}^{-1}$
- C )  $0.61 \times 10^{-3} \text{ erg cm}^{-2} \text{ s}^{-1} \text{ sr}^{-1}$
- CS)  $0.50 \times 10^{-3} \text{ erg cm}^{-2} \text{ s}^{-1} \text{ sr}^{-1}$

comparison between the flux distributions of H<sub>2</sub>(1,0)S(1)  $\lambda 2.12\mu\text{m}$  in our observations and in those by van der Werf et al. shows only a 10% discrepancy in the absolute flux level.

### 2.3. IRSPEC Observations

IRSPEC (Moorwood et al. 1991) observations of the bar using the ESO NTT telescope were carried out in 1991 by Dr A. Moorwood. The detector was a SBRC 62x58 InSb array with pixels of  $\simeq 5\text{\AA}$  (H band ) along the dispersion and  $2''2$  along the slit direction. The slit,  $4''4 \times 120''$  in size, was oriented NE-SW as shown in Fig 1. The data were uncalibrated and in this paper, we merely make use of the profiles of line intensity along the slit.

### 3. Results

In Figs. 2, 3, 4, we show sample spectra averaged over three portions of slit positions 1 and 2 (see Fig. 1). Based on the profiles of line intensity along the N-S direction, we decided to divide the combined slit into three sections which we named *A* (a 28 pixel section to the north), *B* (14 pixels in a central region), and *C* (28 pixels to the south). These sections are displayed in the left panel of Fig. 1. The hydrogen and helium recombination lines peak in position *A* and become weaker to the south whereas the molecular hydrogen lines become stronger and reach their maximum intensity in position *C*. However, there is clearly ionized gas towards the region *C* and vice-versa. In Figs. 2, 3, 4, we show also the spectra summed over 40 pixels in slit position 3 (the ‘‘CS peak’’).

In Table 1, we give intensities corresponding to the spectra shown in Figs. 2, 3 4. They have been averaged over the respective apertures. Line intensities, in each region, are given relative to Br $\gamma$  (put equal to 100). Typical uncertainties vary from  $\simeq 10\%$  for strong lines ( $I \gtrsim 10$ ) to  $\simeq 20\%$  for lines with  $1 \lesssim I \lesssim 10$  and about 50% for the others. When comparing lines in two different bands, a 20% error due to spectrophotometric calibration must also be taken into account.

The line intensities can be corrected for reddening using the Cardelli et al. (1989) prescription  $A_\lambda/A_V = 0.48\lambda_\mu^{-1.61}$ , where we have adopted  $R=5.5$ , as appropriate for the Orion region. From the ratio Pa $\beta$ /Br $\gamma$  we derive  $A_V \sim 2$  mag (Sect.3.2). Note that this value applies only to lines forming in the ionized gas.

The variation in intensity along the amalgamation of slit positions 1 and 2 of a variety of interesting line tracers is shown in Figs. 5 to 7. Figure 8 shows intensity variations in a number of lines from the IRSPEC data. Figure 9 plots the intensity profile of selected lines at slit position 3. From Figs. 5-7, we can see that region *A* coincides roughly with a peak in the lines of HI, which have a second peak in *B*, while the emission of molecular hydrogen has a strong peak in *C* and a weaker one in *B*. Lines of FeII and

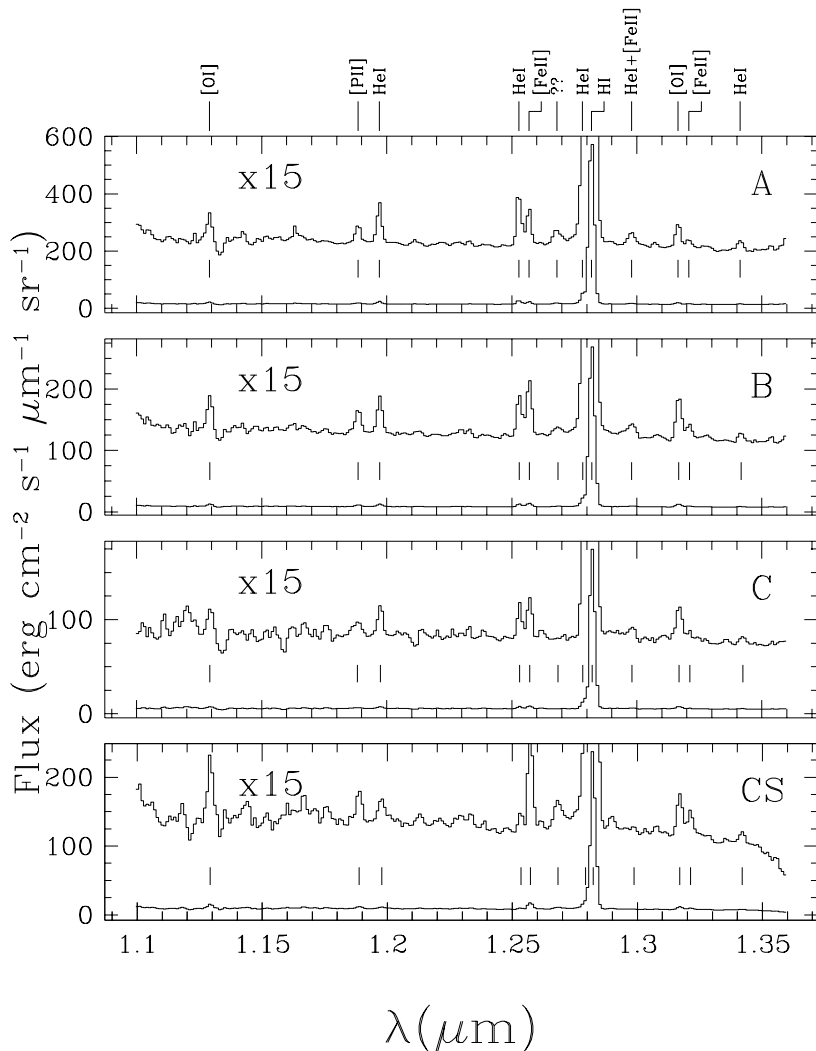


**Fig. 2.** J band spectrum obtained towards the three slit sections *A*, *B* and *C* and in the *CS* position shown in Fig.1. The upper spectrum in each panel has been multiplied by 15 to emphasize weak features.

OI have a sharp peak in *B* and a secondary one in *A*, but are absent in region *C*. In the following, we will use the definition *A*, *B* and *C* (see caption to Fig. 5) both to identify the peaks in the intensity profiles and with reference to Table 1.

We now summarize our results starting with the IRSPEC data which have the advantage that the slit is oriented perpendicularly to the bar. We then discuss in turn the hydrogen and helium recombination lines (which we presume form in the ionized gas), the two oxygen transitions, the collisionally excited iron lines which may form close to the ionization front, and the molecular hydrogen lines which are thought to form in hot neutral gas close to the ionization front.

### 3.1. IRSPEC cut

The observations made using IRSPEC provide a useful introduction to the TIRGO results which have a wider spectral coverage. Figure 8 compares profiles in the Br12 line from the ionized gas, in the FeII  $1.644\mu\text{m}$  ( $4s^4D_{7/2}-3d^7a^4F_{9/2}$ ) line which traces gas close to the ionization front (see below), and in the molecular hydrogen  $v=1-0$  S(1) line from hot ( $T > 1000\text{K}$ ) molecular gas. Figure 8 demonstrates the fact that the molecular hydrogen peak is offset  $\sim 16''$  (0.035 pc) from the ionization front as marked by FeII (or by the fall-off in Br12). The simplest explanation of this (see Tielens et al. 1993, van der Werf et al. 1996) is that one is observing an edge-on PDR and that the observed offset corresponds to the difference between the ionization front where Lyman continuum photons are absorbed and the  $\text{H}_2$  dissociation front where photons ca-

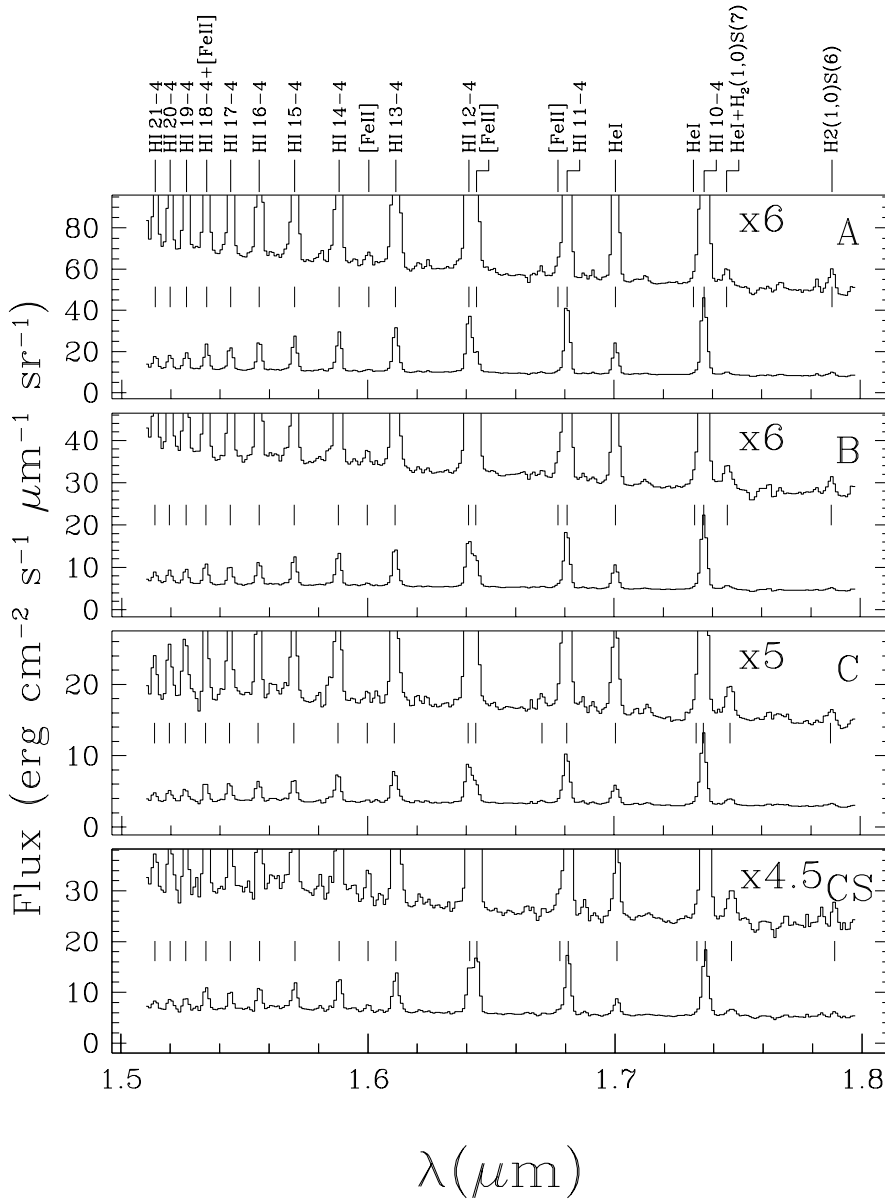


**Fig. 3.** H band spectrum.

pable of dissociating molecular hydrogen are absorbed. We note also that an offset of  $16''$  in the IRSPEC data corresponds (given the orientation NE-SW of the bar) to  $23''$  in the TIRGO slit oriented N-S.

### 3.2. HI lines

In the LONGSP data, we detect many recombination lines of atomic hydrogen, 13 lines of the Brackett series ( $\text{Br}\gamma$  in the K band and 12 lines, from (10-4) to (21-4) in the H band), and  $\text{Pa}\beta$  and  $\text{Pa}\gamma$  in the J band.

We use the 13 lines in the Brackett series to check the accuracy of our data. Figure 10 plots the ratio  $(n-4)/(13-4)$  as a function of the quantum number  $n$  and compares

our results with the prediction of recombination theory (Storey & Hummer 1995). The agreement is quite good, well within our estimate of 10-20% for the observational errors.

The ratio of  $\text{Pa}\beta/\text{Br}\gamma$  provides a value of the extinction  $A_V \sim 2$  mag, assuming the reddening curve of Cardelli et al. (1989) and  $R=5.5$ . We detect a slight variation along slit 1+2, from 2.3 mag in *A* to 1.4 mag in *C*. This variation, however, is within our estimated 25% error in this line ratio. The value in the CS position is  $A_V=1.6$  mag. Figure 10 shows as a dashed line the theoretical line ratios corrected for  $A_V=2$  mag.

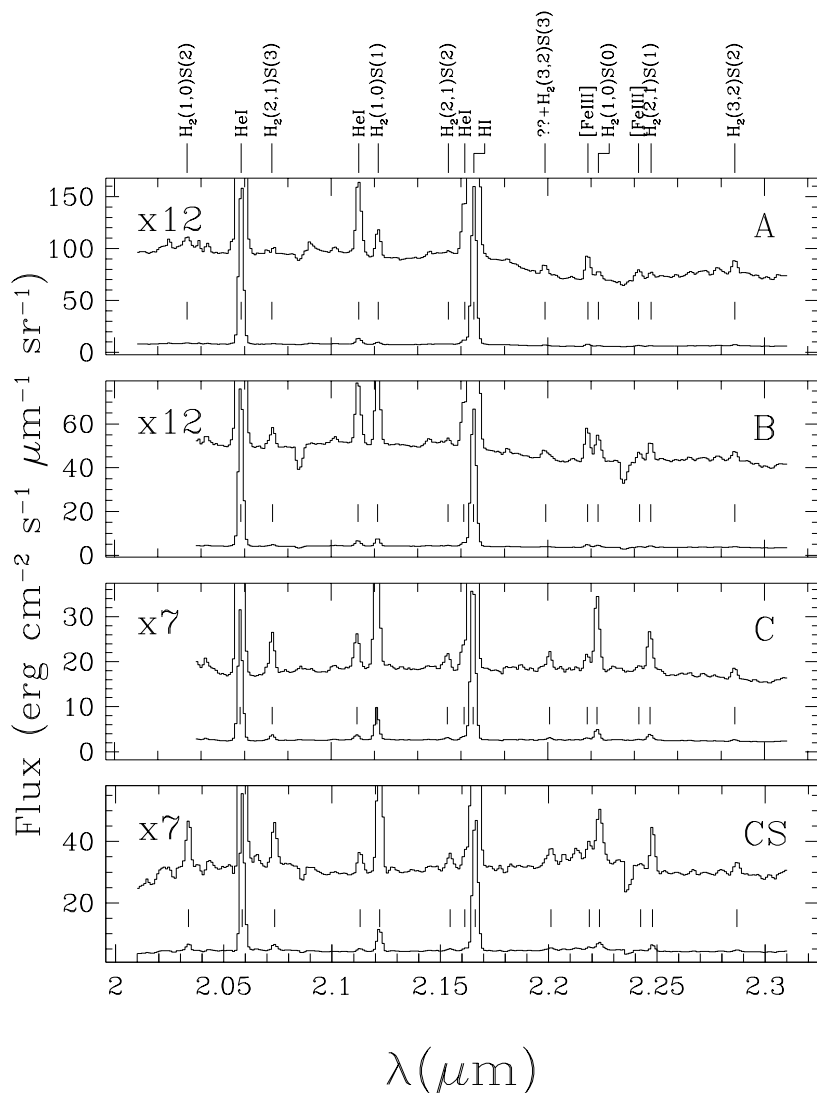


**Fig. 4.** K band spectrum.

### 3.3. He lines

One of the aims of our observations was to examine the extent to which helium is neutral within the zone of ionized gas. Estimates of the helium abundance based upon measurements of either radio or optical recombination lines often assume that the helium and hydrogen Strömgen spheres are coincident with one another (see e.g. Mezger 1980). Our profiles along the slit allow us to make a direct comparison of the HeI and HI line intensities which can then in principle be transformed into the abundance ratio  $[He^+]/[H^+]$  in the immediate vicinity of the ionization front of the Bar.

The chief obstacle in doing this is the uncertainty in helium line intensities which results from collisional excitations from the metastable  $2^3S$  and  $2^1S$  states. Smits (1996) has computed helium line intensities in an approximation where collisions (and self-absorption) out of the

metastable levels into  $n=3$  and  $4$  are neglected although collisions between the  $n=2$  levels are considered. We have compared our observed intensities with Smits predictions for electron density  $10^4 \text{ cm}^{-3}$  and temperature  $10^4 \text{ K}$ . We normalise for this purpose to the  $1.701 \mu\text{m } 4^3D-3^3P^\circ$  transition which has the same upper level as the  $4471 \text{ \AA}$  line often used in optical analyses. It is expected that this transition (see Osterbrock et al. 1992) is only affected at the 1-2 percent level by the collisional effects mentioned above and we neglect such effects in the following. One finds then that, relative to  $4^3D-3^3P^\circ$ , lines such as  $5^3D-3^3P$  are in good agreement with the Smits predictions but  $4^1S-3^1P^\circ$  and  $5^1S-3^1P$  at  $2.113$  and  $1.341 \mu\text{m}$  respectively are factors of roughly 3 stronger. The reason for this may be the neglect of the collisional effects and trapping discussed above (see e.g. Robbins & Bernat 1973; Peimbert & Torres-Peimbert 1977). We in any case have assumed

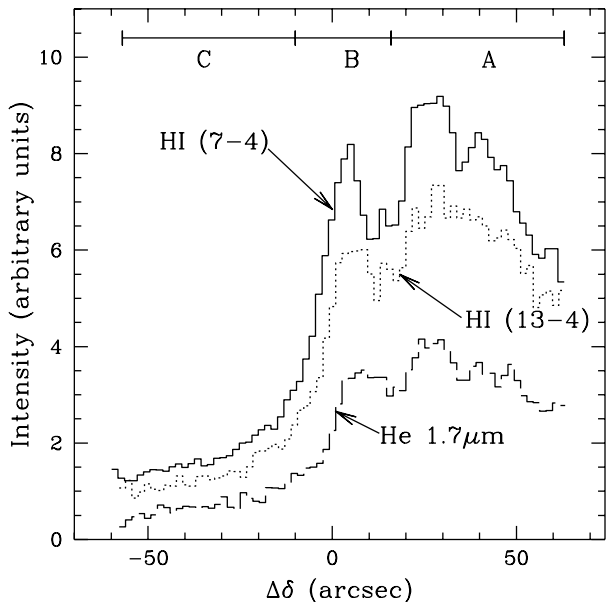


**Fig. 5.** Variation with declination offset (relative to declination (1950) =  $-05^{\circ} 24' 51''$ ) of line intensities measured in the amalgamation of slit positions 1 and 2. The lines are H (7-4) (Br $\gamma$ ; solid), H 13-4 (dotted), and the He line at  $1.701 \mu\text{m}$  (dashed). The vertical scale is arbitrary. We note that regions A, B, and C discussed in the text are defined as follows: A,  $\Delta\delta > 16''$ , B,  $-10'' < \Delta\delta < 16''$ , C,  $\Delta\delta < -10''$ .

that the  $1.701 \mu\text{m}$  line behaves essentially as predicted by the Smits models and can be used to estimate the He<sup>+</sup> abundance. It is natural to compare the He  $1.701 \mu\text{m}$  intensity with that of the adjacent Br10 line. With the above assumptions, we find that :

$$F(\text{He}, 1.7\mu)/F(\text{H}, 10-4) = 3.61 \frac{[\text{He}^+]}{[\text{H}^+]} \quad (1)$$

In Fig. 11, we show the profiles along the slit of the abundance ratio  $[\text{He}^+]/[\text{H}^+]$  deduced from Eq.(1) as well as the ratio of the  $2.06 (2^1\text{P}^o-2^1\text{S})$  to the  $1.7 \mu\text{m}$  lines. The Br $\gamma$  profile along the slit is shown for comparison. We derive an abundance ratio of  $0.093 \pm 0.005$  over region A consistent with He abundance estimates from other authors (see e.g. Baldwin et al.1991 who find 0.088 based on optical measurements and the review of Mezger 1980 (his Fig.5) who shows that radio estimates at positions less than  $100''$  from  $\Theta^1\text{C Ori}$  are in the range 0.083-0.09). It appears that at the position of our slit, the helium and hydrogen Strömgren spheres are close to being coincident. We note with interest the decrease of  $[\text{He}^+]/[\text{H}^+]$  to values of  $\sim 0.075$  in the southern part of the slit or effectively in zone C, where we seem to observe different ionization

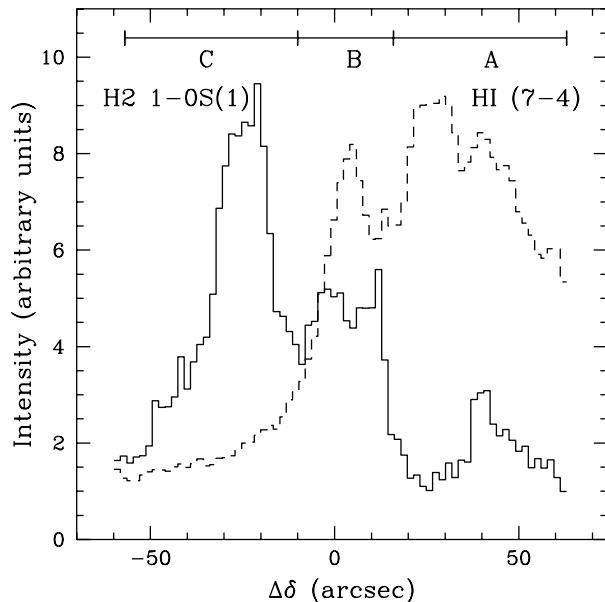


**Fig. 6.** Variation with declination offset of H (7-4) (dashed line) and H<sub>2</sub>(1-0)S(1) (solid line), measured in the amalgamation of slit positions 1 and 2. The regions defined as A, B, and C are shown.

conditions in this (presumably) foreground ionized material. One notes also the fact that the degree of “enhancement” of the  $2.06 \mu\text{m}$  line seems to increase slightly (by a factor of 1.3) in zone C.

### 3.4. OI lines

We detect two OI lines in the J band, the  $2p^33\text{D}-2p^33\text{P}$  at  $1.129 \mu\text{m}$  and the  $2p^34\text{S}-2p^33\text{P}$  at  $1.317 \mu\text{m}$ , with comparable intensity. These lines are produced in the neutral gas by excitation of OI to the upper level of the transitions by UV photons, at  $1027$  and  $1040 \text{ \AA}$  respectively, followed by radiative decay. The fact that the two lines have similar intensity (though not at the CS peak, see Fig.2) suggests that the contribution of Ly- $\beta$  photons to the excitation of the  $2p^33\text{D}$  level (the upper level of the  $1027 \text{ \AA}$  line) is negligible. That the excitation mechanism is fluorescence is confirmed by the spatial variation of the line intensities, which peak at the edge of the ionized region as marked by the HI recombination line emission (cf. Fig. 7). In other words, the oxygen lines are an excellent marker of the ionization front. More precisely, one can say that due to the rapid charge exchange of OI with H<sup>+</sup> and the fact that the hydrogen and oxygen ionization potentials are close to being identical, the oxygen lines trace neutral gas close to the ionization front.



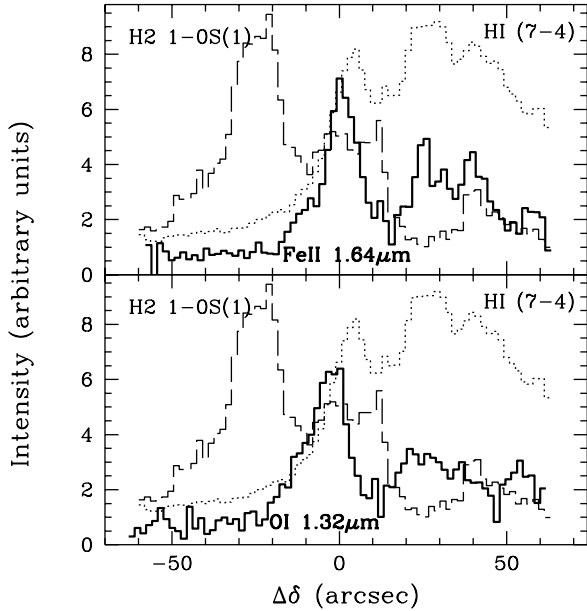


**Fig. 7.** Top panel: variation with declination offset of H (7-4) (dotted line), H2 1-0S(1) (dashed line) and FeII 1.644  $\mu\text{m}$  (solid line). Bottom panel: variation with declination offset of H (7-4) (dotted line), H2 1-0S(1) (dashed line) and OI 1.317  $\mu\text{m}$  (solid line). In both cases, the variations are measured in the amalgamation of slit positions 1 and 2.

It is possible to use the OI lines to derive a measure of the UV radiation field  $G_0$  at the edge of the bar. If fluorescence is the dominant excitation mechanism, the number of photons emitted in the IR line equals the number of photons absorbed by the UV line. Since the optical depth of the UV lines is always very large ( $\tau_0 \sim 5 N/10^{18}$  for the 1040  $\text{\AA}$  line and  $\sim 10 N/10^{18}$  for the 1027  $\text{\AA}$  where  $N$  is the atomic H column density and we have assumed a velocity dispersion  $\Delta v = 3 \text{ km s}^{-1}$  and  $O/H = 6 \times 10^{-4}$ ), the number of absorbed UV photons is proportional to the line equivalent width in the “flat” portion of the curve of growth. This is given by:  $W_\lambda/\lambda_{UV} \sim 1.2 \Delta v/c F(\tau_0) \sim 3.6 \times 10^{-5}$  (Spitzer 1978, p53, where  $\tau_0$  is the UV line center optical depth and  $F(\tau_0) \sim 3$  for optical depths of order 1000). Since both UV lines are in fact triplets with separation larger than  $W_\lambda$ , the total number of UV photons absorbed and re-emitted in each IR line is given by:

$$I_\nu^{UV} = \frac{4\pi \sin \theta_t}{3} \frac{\lambda_{IR} \lambda_{UV}}{c W_\lambda} I(IR) \quad (\text{erg cm}^{-2} \text{s}^{-1} \text{Hz}^{-1}) \quad (2)$$

where  $I(IR)$  is the observed intensity of the IR line in  $\text{erg cm}^{-2} \text{s}^{-1} \text{sr}^{-1}$  and  $\theta_t$  is the angle between the PDR and the line of sight ( $\theta_t = 90$  deg in a face-on PDR; see

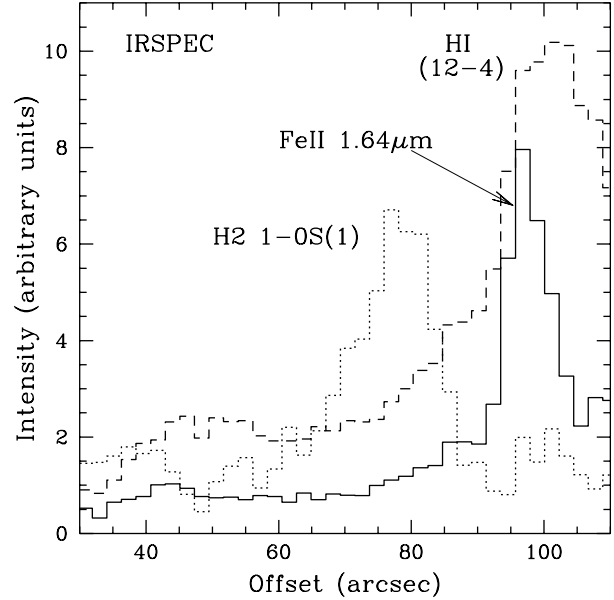


**Fig. 8.** IRSPEC cuts: HI (12-4) (dashed line), H2 1-0S(1) (dotted line) and FeII 1.644  $\mu\text{m}$  (solid line).

Appendix). Note that the three components of the IR lines are not resolved in our spectra.

Equation 2 gives  $I_\nu^{UV} \sim 1.2 \times 10^{-13} \sin \theta_t$  for  $I(IR) = 2.6 \times 10^{-4} \text{ erg cm}^{-2} \text{ s}^{-1} \text{ sr}^{-1}$ , as observed in the main peak of the 1.317  $\mu\text{m}$  line. Here, we have corrected for 2 magnitudes of visual extinction (see Sect. 3.2). The inferred UV intensity can be compared to the flux from  $\Theta^1\text{C Ori}$  at the projected distance of the bar ( $I_p \sim 4 \times 10^{-14} \text{ erg cm}^{-2} \text{ s}^{-1} \text{ Hz}^{-1}$  for  $T_* = 40000\text{K}$ ,  $L_* = 2.5 \times 10^5 L_\odot$ ). The main uncertainty is the appropriate value for  $\theta_t$  but the Orion Bar is known to be close to edge on (see e.g. Hogerheijde et al. 1995). A plausible value is  $\sin \theta_t \sim 0.2$  ( $\theta_t \sim 10 - 15$  deg; see Sect. 3.6), and one finds then that the physical distance of the bar from  $\Theta^1\text{C Ori}$  is about  $(I_p/I_\nu^{UV})^{0.5}$  or 1.3 times the projected distance.

The UV intensity can be expressed relative to the interstellar diffuse field taken here to be  $3 \times 10^7 \text{ photons cm}^{-2} \text{ s}^{-1}$ . The normalized UV intensity is then  $1.3 \times 10^5 \sin \theta_t$  or  $G_0 \sim 2.6 \times 10^4$  (for  $\sin \theta_t = 0.2$ ), similar to the value used by Tielens et al. (1993).

The second, weaker peak of emission  $A$  at  $\Delta\delta \sim 23$  arcsec has an OI intensity about two times lower than the main peak. This may be due to a different orientation of the front with respect to the line of sight. The OI intensity on the CS peak is about 1/4 that of the main peak which again may be due to an orientation effect although it could also imply dust extinction between the CS peak and the

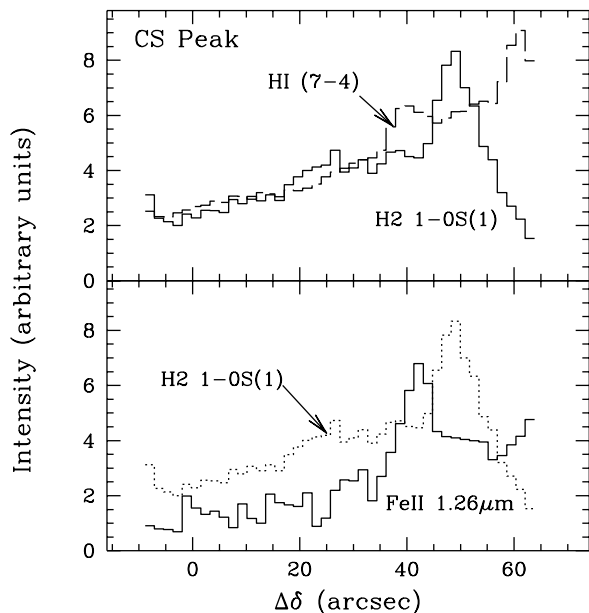


**Fig. 9.** Variation with declination offset along the slit centered on the CS peak of selected lines: HI (7-4) (dashed line, top panel), H2 1-0S(1) (solid line, top panel and dotted line, bottom panel), and FeII 1.257  $\mu\text{m}$  (solid line, bottom panel).

Trapezium. In general, our OI results imply  $G_0$  values at the ionization front in the range  $6000 - 3 \times 10^4$ .

### 3.5. Iron lines

Model calculations suggest (see Baldwin et al. 1991, Rubin et al. 1991, Osterbrock et al. 1992) that iron is mainly in the form FeIV in the Orion nebula. It follows that one expects to see FeII and FeIII emission predominantly at the edge of the Strömgren sphere close to the ionization front. In Fig. 7, we show profiles along our amalgamated slit of the 1.644  $\mu\text{m}$  [FeII] transition compared with the 1.317  $\mu\text{m}$  OI line discussed in the previous section. One sees that the two lines show rather similar behavior with a peak slightly offset from one of the maxima observed in the H recombination lines. It seems plausible that this approximate coincidence denotes the presence of an ionization front and the OI data which we discussed above confirm this idea. It is notable also that the iron lines show no evidence for a coincidence with the molecular hydrogen 1-0 S(1)  $C$  peak at  $\Delta\delta = -27''$  which is also shown on Fig. 7. In fact, our data suggest that both the FeII and FeIII emission lines form in ionized (or partially ionized but not neutral) gas close to the ionization front. It is worth noting here that extinction estimates which we have made using the ratio of the 1.644  $4sa^4D_{7/2} - 3d^7a^4F_{9/2}$  to the 1.26  $\mu\text{m}$   $4sa^4D_{7/2} -$

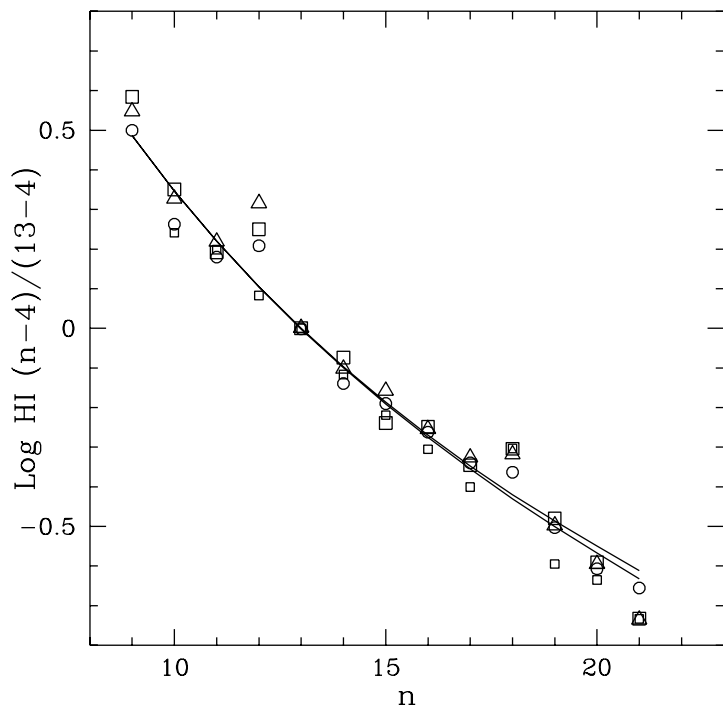


**Fig. 10.** Ratio of the H-band hydrogen recombination lines (n-4)/(13-4) as a function of the quantum number  $n$ . Filled circles refer to position A, triangles to B, squares to C, and diamonds to position CS (the CS peak). The line (18-4) is blended with an [FeII] line. The solid line shows the predictions of recombination theory (Case B). The dashed line shows the Case B ratios corrected for a reddening of  $A_V = 2$  mag.

$4sa^6D_{9/2}$  transitions is consistent with a visual extinction of  $2.7 \pm 0.9$  magnitudes at all positions.

We can estimate the conditions required to explain the relative intensities of the FeII lines. FeII line ratios can be used as indicators of electron density (see Oliva et al. 1990, Pradhan & Zhang 1993). Our most useful indicator appears to be the ratio of the 1.600  $4sa^4D_{3/2} - 3d^7a^4F_{7/2}$  line intensity to that of the 1.644  $4sa^4D_{7/2} - 3d^7a^4F_{9/2}$ . We find that this ratio varies in the range 0.06-0.1 (see table 1) over the regions covered by our slit. Based on the collisional rates of Pradhan & Zhang (1993) (see also Oliva et al. 1990), we conclude that this corresponds to an electron density  $n_e$  of  $4000 \text{ cm}^{-3}$  in the region A),  $6000 \text{ cm}^{-3}$  in region C, and  $3000 \text{ cm}^{-3}$  in region B. At the CS peak position, the observed 1.600/1.644 ratio is 0.12 corresponding to  $n_e = 10^4 \text{ cm}^{-3}$ . Thus, we can exclude high density clumps with  $n_e = 10^6 \text{ cm}^{-3}$  of the type discussed by Bautista et al. (1994). On the contrary, the FeII data seem consistent with ionized gas of electron density  $\sim 10^4 \text{ cm}^{-3}$  or less in the vicinity of the ionization front. It is worth stressing here that this line ratio converges to the LTE value at electron densities of roughly  $10^5 \text{ cm}^{-3}$  and so the lack of high density clumps is significant. More-

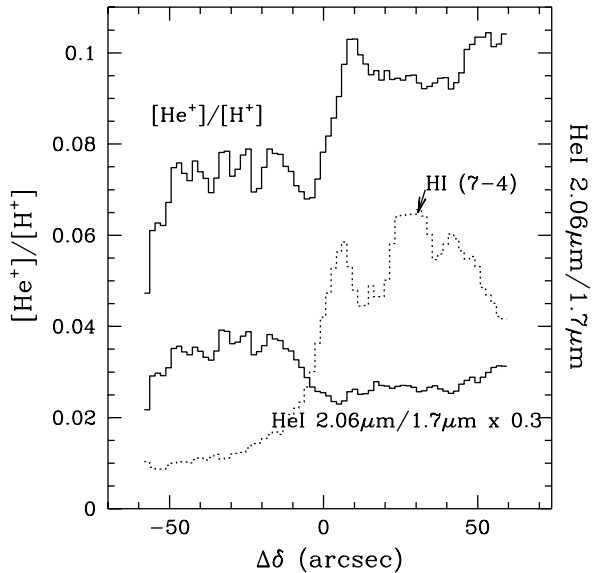


**Fig. 11.** The figure shows the He abundance  $[\text{He}^+]/[\text{H}^+]$  and the ratio of the two HeI lines at 2.058 and 1.701  $\mu\text{m}$  as a function of the declination along the amalgamation of slits 1+2, compared with the  $\text{Br}\gamma$  profile. The data have been smoothed over three pixels.

over, the ionization degree in the layer where the FeII lines are formed is unlikely to be much smaller than unity and hence the hydrogen density is also likely to be of order  $10^4 \text{ cm}^{-3}$ .

### 3.6. $\text{H}_2$ lines

We measured the intensity of 8  $\text{H}_2$  lines in the K band, covering an excitation range from 6472 to 18089 K (see Table 1). Using the data from table 1 and transition probabilities from Turner et al. (1977), we have determined upper level column densities at positions *A*, *B*, *C* and *CS*. In Fig. 12, we plot the column densities per sub-level derived in this manner against excitation energy. One sees that there are clear departures from an LTE distribution suggesting either that fluorescence is playing a role in determining level populations or that there is a sharp gradient of temperature along the lines of sight sampled. The “best fit temperatures” derived from fitting a Boltzmann population distribution to the data in Fig. 12 are moreover rather high with values ranging from  $\sim 2500$  K in region *C* to 3000 K in region *A*.

The high excitation temperatures as well as the (probable) detection of lines from levels as high as  $v=3$  suggest that we are detecting extended fluorescent emission (seen

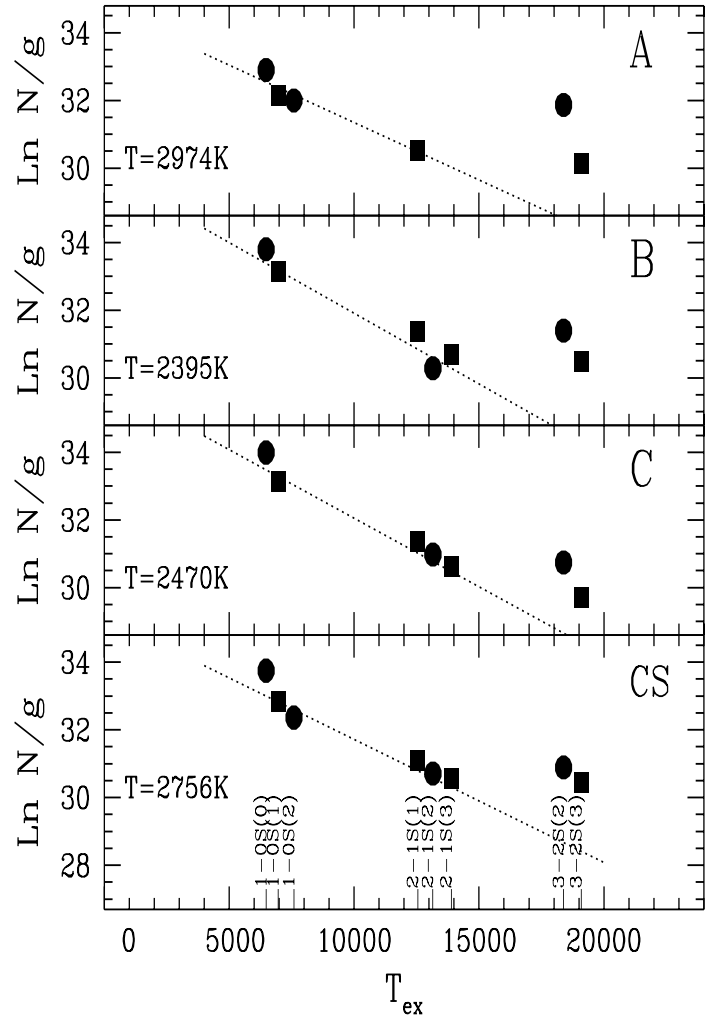


**Fig. 12.** Column density per sub-level against excitation energy of the level at positions *A*, *B*, *C* and on the *CS* Peak. The dotted lines show the best fit to a single temperature population. The two  $v=3$  transitions are doubtful and have not been considered on the fit. Filled squares represent ortho transitions and circles para transitions.

on larger scales by Luhman & Jaffe, 1996) in addition to a “thermal” layer.

The evidence that some fluorescent emission is present is strengthened by the behaviour of the intensity ratio of the  $v=1-0$  S(1) (2.12  $\mu\text{m}$ ) and  $v=2-1$  S(1) (2.25  $\mu\text{m}$ )  $\text{H}_2$  lines along our amalgamated slit (*A*, *B*, *C*), shown in Fig. 13. In a pure fluorescent model, this ratio is predicted to be  $\sim 2$ , whereas an admixture of collisional excitation leads to higher values (12 for pure thermal emission at 2000 K). Our results are consistent with those of van der Werf et al. (1996) in that at the main molecular hydrogen intensity peak *C*, the ratio is  $\sim 6-7$ . A similar value is also found at the secondary peak *B*, which is about coincident with the position of the ionization front as traced by the

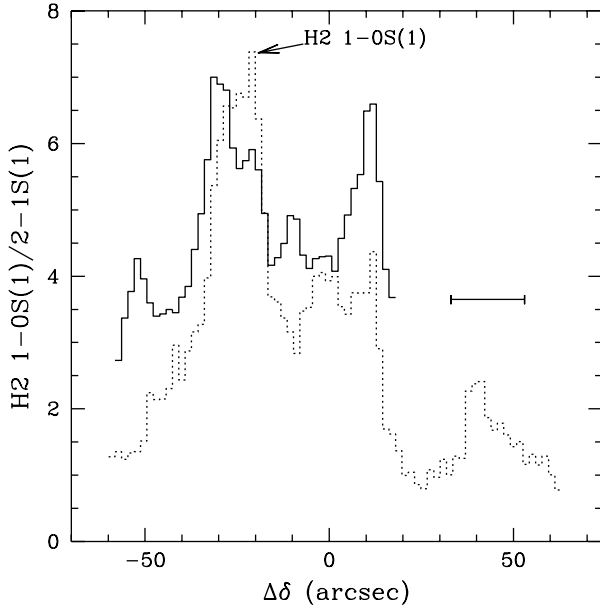


**Fig. 13.** Ratio of the 1-0S(1) to 2-1S(1) H<sub>2</sub> lines as a function of the declination offset along our amalgamation of slits 1+2 (solid line). To compute the ratio, the profiles have been smoothed over three pixels. The horizontal bar shows the value averaged over declination offset 0-50 arcsec. We show for comparison the profile of the 1-0S(1) line (dotted line).

OI lines. Over the rest of the slit the ratio is  $\lesssim 4$ . Thus the fraction of fluorescent emission is smaller at the peaks of  $v=1-0$  S(1) emission.

These measurements, as well as the observed intensity of the  $v=1-0$  S(1) line, can be compared to the PDR model calculations of Hollenbach & Natta (1995) (at steady state). Figure 15 shows the predicted intensity of the 1-0 S(1) line in a face-on PDR as a function of the density for different values of  $G_0$ , and in Panel (2) the ratio of the 1-0 S(1) to the 2-1 S(1) line. In the main molecular peak *C*, we observe a peak intensity of the 1-0 S(1) line of  $\sim 2.3 \times 10^{-4}$  erg cm<sup>-2</sup> s<sup>-1</sup> sr<sup>-1</sup>, and a ratio of  $\sim 7$ . If we assume that the H<sub>2</sub> lines are produced in a PDR with  $G_0 \sim 3 \times 10^4$  (see Sect. 3.3), this corresponds to a density  $6 \times 10^4$  cm<sup>-3</sup>.

These results assume a face-on PDR and there is good reason to suppose that the Orion Bar is seen edge on (see Jansen et al. 1995b for a discussion of the geometry). The effect of a slant of the Bar on the H<sub>2</sub> lines is complicated by the effects of dust extinction and a brief discussion is given in the appendix. The results are different for the vibrationally excited H<sub>2</sub> lines at 2  $\mu$ m and for lines at longer wavelengths, for which the extinction is negligible. Par-

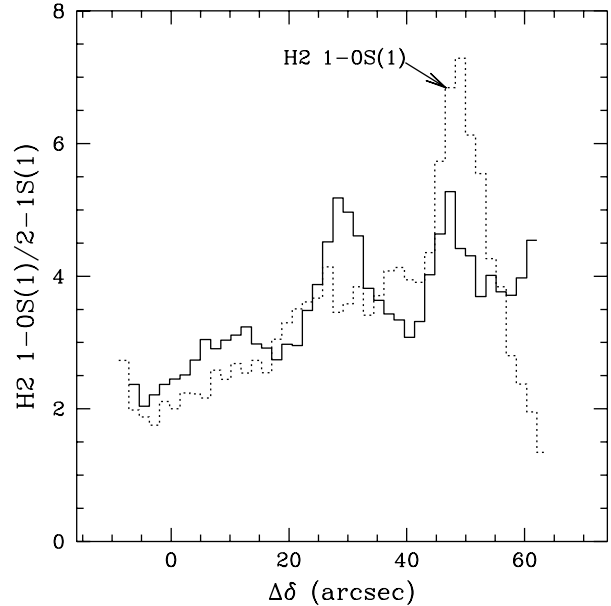


**Fig. 14.** Same as Fig.13 for the CS position.

mar et al. (1991) have observed the J=3-1 (17  $\mu$ m) and 4-2 (12.3  $\mu$ m)  $v=0$  H<sub>2</sub> lines toward the bar and find that their observations are compatible with a hydrogen column density of  $3 \times 10^{21}$  cm<sup>-2</sup> at a temperature of order 500 K. Figure 15 shows in Panel (3) the model-predicted ratio for the two lines observed by Parmar et al. and in Panel (4) the ratio of the  $v=2-1$  S(1) to the J=3-1 (17  $\mu$ m) lines. These ratios can be well reproduced by a model with  $G_0 \sim 3 \times 10^4$  and  $n \sim 6 \times 10^4$  cm<sup>-3</sup> having a moderate enhancement of the intensity of the 12 and 17  $\mu$ m lines due to an inclination of the Bar with respect to the line of sight  $\theta_t \sim 10$ deg. These values are also consistent with the inclination required to explain the intensity of the OI lines, discussed in Sect. 3.4.

The density in the other regions where molecular lines are measured can be estimated in a similar way from Fig. 15. In the secondary molecular peak *B*, assuming the same inclination  $\theta_t \sim 10$ deg, we obtain  $n \sim 4 \times 10^4$  cm<sup>-3</sup>. These densities are a factor of  $\sim 5-10$  larger than that of the ionized gas (see Sect. 3.5) and roughly consistent with the density required to explain the stratification of the bar (i.e the offsets between cold molecular gas and ionization front, see Tielens et al. 1993), which is of order  $5 \times 10^4$  cm<sup>-3</sup>.

Similar densities can be derived from our data at slit position 3, the “CS peak” (*CS*). We show the 1-0 S(1) intensity in Fig. 9 and the  $v=1-0/2-1$  line ratio in Fig. 14. We see a peak of H<sub>2</sub> emission at  $\Delta\delta \sim 49''$  with an intensity

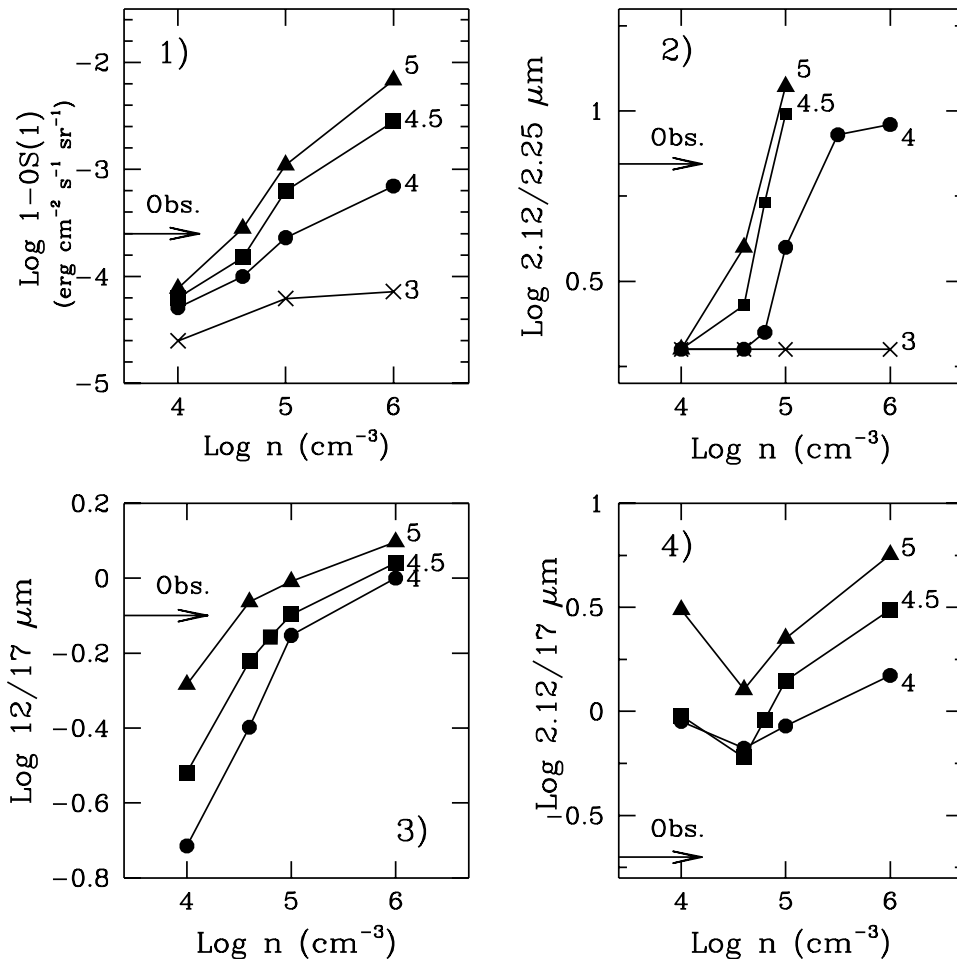


**Fig. 15.** Panel (1): model predictions for the intensity of the  $\text{H}_2$  1-0 S(1) line as a function of hydrogen number density for different values of  $G_0$ . Panel (2): ratio of the  $v=1$ -0 S(1) line at  $2.12 \mu\text{m}$  to the  $v=2$ -1 S(1) line at  $2.24 \mu\text{m}$  as a function of density. Panel (3): ratio of the  $v=0, J=4-2$  line at  $12 \mu\text{m}$  to the  $v=0, J=3-1$  at  $17 \mu\text{m}$ . Panel (4): ratio of the  $v=1$ -0 S(1) line to the  $v=0, J=4-2$ . Each curve is labelled by the logarithm of  $G_0$ . Triangles indicate  $G_0 = 10^5$ , squares with  $G_0 = 10^{4.5}$ , circles with  $G_0 = 10^4$ , and crosses with  $G_0 = 10^3$ . The observed value at peak *C* is shown by the arrow in each panel.

of  $\sim 1.6 \times 10^{-4} \text{ erg cm}^{-2} \text{ s}^{-1} \text{ sr}^{-1}$ , and a broader emission between  $0''$  and  $30''$ , with a peak intensity of  $\sim 8 \times 10^{-5} \text{ erg cm}^{-2} \text{ s}^{-1} \text{ sr}^{-1}$ . In both cases the ratio of the two  $\text{H}_2$  lines is about 5 implying densities  $\lesssim 10^5 \text{ cm}^{-3}$  for  $G_0 \sim 10^4$ . Neither of the peaks coincide with the “ionization front” as defined by FeII (Fig. 9). One would expect such a coincidence if the densities were considerably above  $10^5 \text{ cm}^{-3}$  as implied by the CS data (see van der Werf et al. 1996). Thus the general conclusion is that the PDR as seen in molecular hydrogen appears to be at densities below  $10^5 \text{ cm}^{-3}$  in contrast to the millimeter results which suggest the existence of clumps at densities well above  $10^5 \text{ cm}^{-3}$ .

A caveat to much of the above discussion is that comparisons which we have made between the predictions of the Hollenbach & Natta code used by us and other results (in particular, the results of Störzner & Hollenbach 1997) shows that there can be substantial differences in both the

$\text{H}_2$  line intensities and in some line ratios. The main reason for this is the extreme sensitivity of  $\text{H}_2$  line intensities to the temperature structure although there are more minor effects which also play a role (note for example that the Hollenbach Natta models neglect the effects of the carbon oxygen chemistry upon  $\text{H}_2$ ). This has the consequence that rather minor errors in the treatment of thermal equilibrium can affect our conclusions. In this respect, mid infrared intensity ratios such as the 12/17 micron ratio measured by Parmar et al. are important because they afford a direct measure of temperature. Thus if the temperature structure can be adjusted to fit the mid infrared observations, one may have some confidence in the predictions for other lines. For the moment, we conclude that the fact that we have been able to fit the 12/17 ratio suggests that the model which we have used is reliable.

#### 4. Discussion

Our analysis of molecular hydrogen in the previous section has assumed implicitly that the H<sub>2</sub> emission comes at all positions from material heated by the stellar radiation field (PDR). The two peaks *C* and *B* we observe must then come from two different structures. In fact, there are indications in the molecular hydrogen images of van der Werf et al. that in H<sub>2</sub> lines there are *two* bars. One of these (which one might call the main H<sub>2</sub> bar) corresponds to the feature seen in our Fig. 6 at position *C* ( $\Delta\delta = -24''$ ). The “second H<sub>2</sub> bar” (less well defined in the van der Werf et al. images) is close in projection to the main ionization front and corresponds to the peak in Fig. 6 at  $\Delta\delta = -2''$  (roughly coincident with the OI peak). We propose that these two bars are separated along the line of sight and that the shift in position ( $15''$  accounting for our slit orientation) is due to a tilt in the bar of  $\sim 10$  degrees as discussed above. Thus, the bar is split along its length (essentially along the line of sight) into two sections separated by 0.2-0.3 parsec. Each half of the bar in this scenario has a length of order 0.1 parsec and thus the total length along the line of sight is of order 0.3-0.4 parsec or somewhat smaller than proposed by Jansen et al. (1995b).

There are problems with this model however. The principal difficulty is that our data do not show evidence for ionization front indicators (OI and FeII) roughly coincident (one expects a shift of order 6 arc second for a density of  $5 \times 10^4 \text{ cm}^{-3}$ ) with the main ( $\Delta\delta = -24''$  on our slit) molecular hydrogen peak. One explanation for this might be that the density in the layer of gas between the ionization and H<sub>2</sub> dissociation front is a factor of 2-3 lower (of order  $2 \times 10^4 \text{ cm}^{-3}$ ) and thus that the main H<sub>2</sub> peak is shifted  $15''$  ( $20''$  in our NS oriented slit) relative to the main ionization front (i.e., peak *C* in H<sub>2</sub> corresponds to peak *B* in OI). Equally, the ionization front emission seen in Fig. 7 at  $\Delta\delta = 23''$  might correspond to the H<sub>2</sub> emission at  $\Delta\delta = 3''$ . This lower density between ionization and photo-dissociation fronts implies a density increase between the atomic and molecular regions by at least a factor of 4 since the general bar stratification requires an average density of at least  $5 \times 10^4 \text{ cm}^{-3}$  in order to account for the observed offsets of ionization front and molecular lines (see also Wyrowski et al. 1997).

Thus, one possible interpretation (see also Simon et al. 1997) of the H<sub>2</sub> data is that there is a sharp density gradient perpendicular to the line of sight such that the molecular gas has much higher density than the partially ionized atomic medium adjacent to it. This has the attractive feature that it helps explain one of the puzzles concerning the bar which is the discrepancy (more than an order of magnitude) between the hydrogen column density derived by Parmar et al. (1991) and that inferred by Hogerheijde et al. (1995) from their C<sup>18</sup>O data. The Parmar et al. data refer essentially to the main H<sub>2</sub> bar whereas Hogerheijde et al. preferentially sample the fully molecu-

lar gas to the SE. A density gradient may also cause the offset between the ionization front and the main molecular hydrogen peak to be larger than that estimated using a homogeneous model whereas molecular hydrogen and carbon radio recombination lines would become closer to one another.

This last aspect is particularly interesting in view of the coincidence found by Wyrowski et al. (1997) between the bar seen in C91 $\alpha$  emission and the main H<sub>2</sub> bar. The difficulty in explaining this result stems from the fact that one expects the H<sub>2</sub> emission to come from gas with temperature above 2000 K while the carbon line is thought to be formed at temperatures which are considerably lower. In fact, there is a firm upper limit of 1600 K on the temperature of the gas responsible for the C91 $\alpha$  emission (based on the line width). The proposed density gradient discussed above may cause the offset between the photodissociation front (i.e H<sub>2</sub> emission) and carbon line emission to diminish.

A different interpretation of our observations is in principle possible. Our main molecular hydrogen peak *C* at  $\Delta\delta = -24''$  could be produced by a low velocity shock preceding the ionization front. This would explain the lack of ionization front indicators coincident with molecular hydrogen. However, the kinematics of the emission seen in C91 $\alpha$  by Wyrowski et al. are difficult to explain in this scenario. One needs a shock velocity of at least  $3 \text{ km s}^{-1}$  to excite H<sub>2</sub> (see Tielens et al. 1993) and then the observed C91 $\alpha$  line widths become difficult to understand.

It is intriguing that our H<sub>2</sub> observations do not show any evidence of high density gas. This is in contrast with the fact that the molecular line data (e.g. Tauber et al. 1995, Simon et al. 1997, van der Werf et al. 1996) give evidence for a considerable fraction of the gas being in clumps with density  $\gg 10^5 \text{ cm}^{-3}$ . Such clumps can be expected to affect our results because most of the lines observed by us are sensitive to high emission measure and high density. High density PDRs are expected to be hotter and hence considerably more intense in H<sub>2</sub> v=2-1 and 1-0 emission than lower-density PDRs (cf. Fig. 15). Nevertheless, our data show no evidence for gas with density above  $10^5 \text{ cm}^{-3}$  even towards regions where Simon et al. (see also van der Werf et al.) estimate molecular hydrogen densities of order  $2 \times 10^5 \text{ cm}^{-3}$ . We see no reason on the other hand why clumps should dissipate on a short timescale when traversing the H<sub>2</sub> dissociation front and suggest therefore that clumps, while possibly present, are a secondary phenomenon.

More important in our opinion is the density gradient mentioned above. It is worth noting that in the scenario which we are advocating, the thermal pressure may be constant (at a value of the order of  $10^8 \text{ cm}^{-3}\text{K}$ ) along a line perpendicular to the bar and we conclude that isobaric models of the Bar are worth examining. This incidentally would suggest relatively low values for the magnetic pressure and hence magnetic field (below 0.5 mG).

## 5. Conclusions

This study has presented NIR slit spectra of the Orion Bar region. Our main result is based on the molecular hydrogen line intensities and is that the densities derived from these tracers are of order  $3 - 6 \times 10^4 \text{ cm}^{-3}$  and thus consistent with estimates of the mean density derived from the observed stratification of the bar (e.g. Tielens et al. 1993, Wyrowski et al. 1997). Comparison with the longer wavelength  $\text{H}_2$  data of Parmar et al. (1991) implies a tilt for the bar relative to the line of sight of  $\sim 10$  degrees. Our data suggest also that the bar may be split into two portions along the line of sight which are separated by 0.2-0.3 parsec. It seems plausible that the density is lower in the “atomic” region (perhaps  $2 \times 10^4 \text{ cm}^{-3}$ ) than in the molecular gas (of order  $10^5 \text{ cm}^{-3}$ ). We conclude that models with constant thermal pressure should be examined in future studies of the bar region.

We have also derived densities for the ionized gas in the vicinity of the ionization front using [FeII] line ratios and find values of order  $10^4 \text{ cm}^{-3}$ . This together with the molecular hydrogen data has convinced us that high density neutral clumps play a rather minor role in determining the observed characteristics of the bar.

A by-product of these observations was that we were able to use the observed OI line at  $1.317 \mu\text{m}$  as an estimator for the ultraviolet radiation field incident upon the bar. We estimate the normalised FUV intensity  $G_0$  on the bar to be  $0.6 - 3.0 \times 10^4$  using this tracer.

Finally, we have used the  $1.701 \mu\text{m}$  line of He to examine the degree of coincidence of helium and hydrogen Strömgen spheres. To within our errors, we find that  $\text{He}^+$  and  $\text{H}^+$  coexist and hence that He abundance estimates using these tracers should be reliable.

*Acknowledgements.* We are indebted to D.P. Smits, who provided us with the results of his He level population calculations and J.H. Black for making available to us his  $\text{H}_2$  transition probabilities. Paul van der Werf allowed us to use his  $\text{H}_2$  image of the Bar and Alan Moorwood gave us his IRSPEC data. Special thanks are due to Tino Oliva, for his help and comments on this projects. This work was partially supported by ASI grant 94-RS-152 and GNA grant 96/00317 to the Osservatorio di Arcetri. A.M. acknowledges partial support through GO grant G005.44800 from Space Telescope Science Institute, which is operated by the Association of Universities for Research in Astronomy, Inc., under NASA contract NAS 5-26555.

### A. The effects of inclination on the $\text{H}_2$ lines

The intensity of a given line as a function of the angle  $\theta_t$  can be approximately estimated from the expression (cf. Fig. 16):

$$I = I_0/\tau_0(1 - e^{-\tau})e^{-\tau_n} \quad (\text{A1})$$

where  $I_0$  is the face-on intensity ( $\theta_t = 90$ ) ignoring extinction due to dust,  $\tau$  the dust optical depth at the line

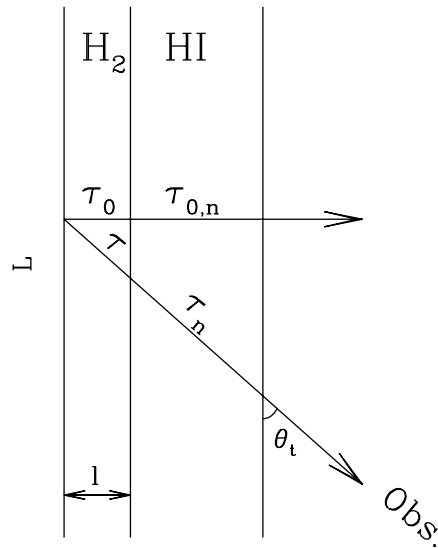


**Fig. 16.** Sketch of the geometry for molecular hydrogen emission discussed in the Appendix. The symbols used in Eq.(A1) are defined. The observer sees the PDR at an angle  $\theta_t$ . The layer of  $\text{H}_2$  emission has continuum optical depth  $\tau_0$  and the foreground atomic layer optical depth  $\tau_{0,n}$ .

frequency across the layer of the PDR which contributes to the  $\text{H}_2$  emission,  $\tau_n$  the optical depth of the HI region along the line of sight.  $\tau_0$  and  $\tau_{0,n}$  are the optical depths in the  $\text{H}_2$  and HI regions, respectively, in the direction perpendicular to the PDR. To first approximation,  $\tau \sim \tau_0/\sin \theta_t$ ,  $\tau_n \sim \tau_{0,n}/\sin \theta_t$ . For  $\theta_t \lesssim l/L$ , the line of sight does not intercept the neutral region of the PDR ( $\tau_n \sim 0$ ) and the line intensity tends to  $I/I_0 \sim 1/\tau_0$ . When  $\tau_0 = \tau_{0,n} = 0$ , then  $I/I_0 = 1/\sin \theta_t$ .

Figure 17 shows the ratio  $I/I_0$  for the 1-0 S(1) line (solid curve), which has been derived using  $\tau_0 \sim 1 \times A_\lambda/A_v$ ,  $\tau_{0,n} \sim 1 \times A_\lambda/A_v$ ,  $A_\lambda/A_v = 0.145$ . Here we assume, based upon models, 1 magnitude of visual extinction in the  $\text{H}_2$  emitting layer and 1 magnitude of extinction in the foreground HI layer. For the 1-0 S(1) line,  $I/I_0 \sim 1$  with an accuracy better than 30% for  $\theta_t \gtrsim 8 \text{ deg}$ . The figure shows also the variation with  $\theta_t$  of the ratio of the 1-0 S(1) line at  $2.12 \mu\text{m}$  to the  $v=0, J=3-1$   $17 \mu\text{m}$  line (for which  $\tau_0 \sim \tau_{0,n} \sim 0$ ), with respect to the same ratio for a face-on PDR.

## References

Baldwin J.A., Ferland, G.J., Martin, P.G. et al. 1991, ApJ 374, 580

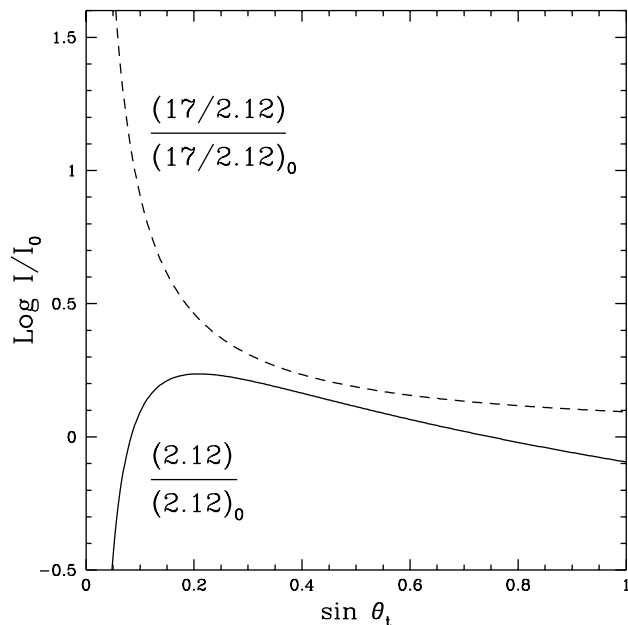


**Fig. 17.** The solid line shows, as a function of the inclination angle  $\theta_t$ , the intensity of the 1-0 S(1) line normalized to the value in a face-on PDR where dust extinction is neglected. The dashed line shows the ratio of the two lines 1-0 S(1) and  $\nu=0$ ,  $J=3-1$  at  $17 \mu\text{m}$ , normalized in an analogous fashion.

Bautista M.A., Pradhan A.K., Osterbrock D.E. 1994, ApJ 432, L135  
 Bautista M.A., Pogge R.W., DePoy D.L. 1995, ApJ 452, 685  
 Bertoldi F., Draine B. 1996, ApJ 458, 222  
 Cardelli J.A., Clayton G.C., Mathis J.S. 1989, ApJ 345,245  
 DePoy D.L., Pogge R.W. 1994, ApJ 433, 725  
 Draine B.T., Bertoldi F. 1996, ApJ 468, 269  
 Dyson J.E., Williams R.J.R., Redman M.P., 1995, MNRAS 277,700  
 Felli M., Churchwell E., Wilson T.L., Taylor G.B. 1993, A&AS 98,137  
 Fuente A., Martín-Pintado J., Cernicharo J., Bachiller R., 1993, A&A 276,473  
 Genzel R. 1992, in "The galactic Interstellar Medium", p275, (Burton W.B., Elmegreen B.G., Genzel R.), Springer  
 Genzel R., Stutzki J. 1989, ARA&A 27,41  
 Glassgold A.E., Huggins P.J., Schucking E.L. (Editors) 1982 *Symposium on the Orion Nebula to honor Henry Draper*, Annals of the New York Academy of Sciences, Vol. 395  
 Hogerheijde M.R., Jansen D., van Dishoeck E.F. 1995, A&A 294, 792  
 Hollenbach D., Takahashi T., Tielens A. 1991, ApJ 377, 192  
 Hollenbach D., Natta A. 1995, ApJ 455,133  
 Hollenbach D., Tielens A. 1997, ARA&A (in press)  
 Hunt L.K., Lisi F., Testi L., et al., 1996, A&AS 115, 181  
 Hunt L.K., Migliorini S., Testi L., et al., 1997, AJ (submitted).

Hunt L.K., Testi L., Borelli S., Maiolino R., Moriondo G., 1994, Technical Report 4/94, Arcetri Astrophysical Observatory  
 Jansen D.J., van Dishoeck E.F., Black J.H., Spaans M., Sosin C. 1995a, A&A 302, 223  
 Jansen D.J., Spaans M., Hogerheijde M., van Dishoeck E.F. 1995b, A&A 303, 541  
 Lisi F., Hunt L.K., Baffa C., et al., 1996, PASP 108, 364  
 Lizano S., Canto J., Garay G., Hollenbach D. 1996, ApJ 468,739  
 Luhman M.L., Jaffe D.T., 1996, ApJ 463,191  
 Mathis J.S. 1995, *Rev Mex AA (Serie de Conferencias)* 3, 207  
 Mezger P.G. 1980 pp81-97 in *Radio Recombination Lines*, P.A.Shaver (ed), publ. D.Reidel, Vol. 80, Astrophys. and Space Science Library  
 Moorwood A.F.M., Monet A., Gredel R., 1991, The Messenger 63, 77  
 Oliva E., Moorwood A.F.M., Danziger I.J. 1990 A&A 240,453  
 Oliva E., Origlia L., 1992, A&A 254, 466  
 Osterbrock D.E., Shaw R.A., Veilleux S. 1990, ApJ 352, 561  
 Osterbrock D.E., Tran H.D., Veilleux S. 1992, ApJ 389, 305  
 Pankonin V., Walmsley C.M., Harwit M. 1979, A&A 75,34  
 Parmar P.S., Lacey J.H., Achtermann J.M. 1991, ApJ 372, L25  
 Peimbert M. 1982 in *Symposium on the Orion Nebula*, edited Glassgold A.E. et al., Annals of New York Academy of Sciences Vol 395, 24  
 Peimbert M. 1993, *Rev. Mexicana de Astron. y Astrof.* 27,9  
 Peimbert M. 1995, p163 in *The Analysis of Emission Lines*, edited R.E.Williams and M.Livio, Space Tel. Science Inst. Series, 8  
 Peimbert M., Torres-Peimbert S. 1977, MNRAS 179, 217  
 Peimbert M., Torres-Peimbert S., Ruis M.T. 1992, *RevMexAA* 24,155  
 Pogge R.W., Owen J.M., Attwood B. 1992, ApJ 399, 147  
 Pradhan A.K., Zhang H.L. 1993, ApJ 409, L77  
 Robbins, R.R., Bernat, A.P. 1973, Mem.Soc.R.Sci. Liege 6th ser., 5, 263  
 Rodriguez M. 1996 A&A 313,L5  
 Rubin R.H., Simpson J.P., Haas M.R., Erickson E.F. 1991, PASP 103, 834  
 Rubin R.H., Dufour R.J., Walter D.K., 1993, ApJ 413,242  
 Simon R., Stutzki J., Sternberg A., Winnewisser G. 1997, A&A (in press)  
 Simpson J.P., Rubin R.H., Erickson E.F., Haas M.R. 1986, ApJ 311, 895  
 Smits D.P. 1996, MNRAS 278, 683  
 Spitzer L. 1978, *Physical Processes in the Interstellar Medium*, publ. J.Wiley & Sons  
 Sternberg A., Dalgarno A. 1989, ApJ 338,197  
 Sternberg A., Dalgarno A. 1995, ApJS 99, 565  
 Storey P.J., Hummer D. 1995, MNRAS 272,41  
 Störzer H., Hollenbach D. 1997, ApJ in press.  
 Tauber J.A., Tielens A.G.G.M., Meixner M., Goldsmith P.F. 1994, ApJ 422,136  
 Tauber J.A., Lis D.C., Keene J., Schilke P., Büttgenbach, T.H. 1995, A&A 297, 567  
 Tielens A., Hollenbach D. 1985, ApJ 291, 722  
 Tielens, A.A.G.M., Meixner, M.M., van der Werf, P.P., Bregman, J., Tauber, J.A., Stutzki, J., Rank, D. 1993, Science 262,86  
 Turner J., Kirby-Docken K., Dalgarno A. 1977 ApJS 35, 281



- van der Werf P., Stutzki J., Sternberg A., Krabbe A. 1996, A&A 313, 633
- Vanzi L., Sozzi M., Marcucci G., et al. 1997a A&AS 124, 573
- Vanzi L., Gennari S., Ciofini M., Testi L., 1997b, Experimental Astronomy, submitted
- Vanzi L., Marconi A., Gennari S., 1995, in “New Developments in Array Technology and Applications”, eds. A.G. Davis Philip et al., p. 231
- Walmsley M. 1997, in Proceedings of the 1<sup>st</sup> Arecibo Workshop on “Molecular Spectroscopy with the upgraded Arecibo telescope in the 1-10GHz range”, editors L.Olmi, W.Baan., in press
- Wilson T.L., Jäger B. 1987, A&A 184,291
- Wilson T.L., Filges L. 1990 in *Radio recombination lines ; 25 years of investigation*, ed. M.A.Gordon, R.L.Sorochenko.
- Wilson T.L., Filges L., Codella C., Reich W., Reich P. 1997, A&A (in press)
- Wyrowski F., Schilke P., Hofner P., Walmsley M. 1997, ApJ 487, L171
- Yusuf-Zadeh F. 1990 ApJ 361, L19